DESIGN OF COMPACT LARGE MOMENTUM ACCEPTANCE SEPARATE FUNCTION MAGNET BEAMLINES FOR PARTICLE THERAPY

S. Barg*[1], J. A. Bellesini[1], S. L. Sheehy[1,2], A. F. Steinberg[1], J. S. L. Yap[1,3]
[1]The University of Melbourne, Melbourne, Australia
[2]Australian Nuclear Science and Technology Organisation, Sydney, Australia
[3]Peter MacCallum Cancer Centre, Melbourne, Australia

Abstract

The University of Melbourne's TURBO (Technology for Ultra Rapid Beam Operation) project aims to improve charged particle therapy by developing large momentum acceptance beamlines to reduce the energy layer switching time, increasing the efficiency of delivery systems for cancer treatment. Previously, a closed-dispersion arc has been designed utilizing non-linear magnets built as Halbach arrays, which achieves up to ±42 % rigidity acceptance in a beamline with an overall bend of 30°. Here – considering the technological complexity of these non-linear magnet arrays – we present a design methodology for compact large momentum acceptance beamlines based on separate-function magnets. We find parameters representing clinical beam quality requirements and perform a multi-objective optimization to investigate trade-offs between them. The separate-function approach provides an alternative for a full-scale beamline that relies on simpler, commercially available technology.

INTRODUCTION

An advantage of charged particle therapy compared to conventional X-ray radiotherapy is the more localized energy deposition due to the characteristic Bragg peak, which limits the exposure of healthy tissue [1, 2]. This increased conformity is especially beneficial for the treatment of cancers in children, or tumors close to critical organs, such as the brain or spinal cord [1, 3]. To access different depths within the patient body, the beam energy needs to be varied. The clinical range for proton therapy is typically 70-230 MeV [2], equivalent to a momentum acceptance of 30 %.

Current beam delivery systems achieve momentum acceptance ranges of 0.5-1 % and thus require magnet ramping [4], resulting in a high energy layer switching time which can contribute more than 70 % to the overall beam delivery time [5]. The efficiency of charged particle therapy could be improved by overcoming this obstacle and utilizing large momentum acceptance (LMA) beamlines.

In the context of the TURBO project, a beam delivery system has been developed that uses fixed-field magnets with many multipole components per magnet to obtain the necessary degrees of freedom to achieve LMA [6]. For this, Halbach arrays [7] are employed, which consist of bars of permanent magnet material that can be oriented in a way that the superposition of their individual fields creates the required combination of multipole contributions. A low-energy (0.5-3 MeV) demonstrator for this technology is currently under construction in the University of Melbourne's Pelletron laboratory.

For up-scaling to clinical energies, we investigate alternative approaches, specifically beamline designs based on simpler technology, such as separate-function (SF) magnets. The number of free parameters per magnet is greater for Halbach arrays, so that a similar momentum acceptance would require more magnets (and space) if implemented via SF components. A study by Nesteruk et al. indicates that for the treatment of 70 % of proton therapy patients at the Paul Scherrer Institute, an acceptance of ±17 % is sufficient [8], which motivates a discussion of the trade-off between technology complexity and achievable beam quality.

In the following, we first express the requirements we impose on an LMA beamline in terms of accelerator physics concepts. Then, we present beam quality metrics relevant to clinical application. Finally, we investigate how these two types of conditions are connected by studying a simple SF magnet beamline as a sample case, which we also use to validate a multi-objective algorithm that can be employed when introducing a greater number of magnets.

Our system needs to be compact and provide bending, since – apart from the beam delivery time – crucial limitations of particle therapy are the availability and cost. Since retrofitting into existing radiotherapy bunkers in hospitals has been identified as a way to mitigate both problems [2], these additional constraints are imposed to reduce the footprint of our beamline.

ACHROMAT CONDITIONS

An LMA arc needs to achieve both geometrical and optical achromaticity, which means that trajectories of particles with different momenta have to converge onto a joined path at the end of the beamline and any initial phase space distribution has to be recovered. Meeting both conditions ensures input-independence and supports a seamless integration of the delivery beamline into the full treatment system. Geometrical achromaticity is obtained if the dispersion D and its derivative D' are zero ($D = 0, D' = 0$) at the start and the end of a beamline, across the full range of momenta [9]. For a beamline with midpoint symmetry, this corresponds to a requirement for the angle to the reference path, which has to hold for all relative momentum deviations $\delta_p = \frac{\Delta p}{p}$ in the horizontal plane at the midpoint:

$$x'_{\mathrm{mid}}(p) = 0.$$

* simon.barg@student.unimelb.edu.au

From this, we can obtain a cost function F_1 for simulations of an LMA beamline by summing over multiple energies E_i within the considered range $[E_{min}, E_{max}]$. For optimizations, this function needs to be minimized:

$$F_1 = \sum_i \left(x'_{\mathrm{mid}}(E_i)\right)^2 . \quad (1)$$

To achieve optical achromaticity by reproducing any initial phase space distribution at the end of the beamline, a phase advance of $n \cdot 2\pi$ for an integer n is required, which can be translated into a condition for the traces of the horizontal and vertical transfer matrices $\mathscr{M}_x$ and $\mathscr{M}_z$. For circular input beams, where a π phase advance achieves the same, this condition is:

$$|\mathrm{Tr}(\mathscr{M}_x)| = |\mathrm{Tr}(\mathscr{M}_z)| = 2,$$

which is used for the second cost function

$$F_2 = (\mathrm{Tr}(\mathscr{M}_{x,0}) - 2)^2 + (\mathrm{Tr}(\mathscr{M}_{z,0}) - 2)^2, \quad (2)$$

which is only evaluated at the reference energy E_0 as this proves more efficient but equally effective in the example presented below.

BEAM QUALITY METRICS

To ensure the suitability for clinical applications, certain beam parameters need to be reproducible [10], both for repeated irradiation with the same energy and across the full energy range. Three metrics relevant for the beamline design are the position, shape and size deviations relative to the beam at reference energy E_0. The maxima of these over the considered energies E_i are expressed as:

$$\text{Position:} \quad d_{max} = \max_{E_i}(d_i) \quad (3)$$

$$\text{Shape:} \quad \epsilon_{max} = \max_{E_i}(\epsilon_i) \quad (4)$$

$$\text{Size:} \quad \delta_{A,max} = \max_{E_i}(\delta_{A,i}) \quad (5)$$

where ϵ_i and $\delta_{A,i}$ are the 'ellipticity' and the size variation relative to the reference energy, respectively. Ellipticity describes how non-circular the beam spot is by comparing its major and minor axes a and b, which are also used to determine the area of the beam spot $A_i = \pi a_i b_i$, so that:

$$\epsilon_i = 2\frac{a_i - b_i}{a_i + b_i}, \quad \text{and} \quad \delta_{A,i} = \frac{A_i - A_0}{A_0}.$$

Compared to tracking a large number of particles, a computationally efficient way of determining a and b in simulations is utilizing their relation to the horizontal and vertical Courant-Snyder (Twiss) beta parameters β_x and β_z – which can be obtained from the transfer matrix – and the emittance ε that we assume to be equal for both planes:

$$a, b = \max, \min\left(\sqrt{\varepsilon\beta_x}, \sqrt{\varepsilon\beta_z}\right).$$

From literature, we find explicit limits for these quality measures at a single energy, which can be used as a lower bound for the allowed variations across the energy range. Liao et al. state that position deviations of up to 5 mm can be corrected by the system that provides the transverse scanning across the tumor, while they determine a maximum ellipticity of 10 % [11]. The American Association of Physicists in Medicine TG 224 quality assurance guidelines recommend size variations less than 10 % compared to baseline [12]. In summary, the explicit limits are:

$$d_{max} = 5\,\mathrm{mm}, \quad \epsilon_{max} = 10\,\%, \quad \delta_{A,max} = 10\,\%.$$

ACHROMAT CONDITION VALIDATION FOR SAMPLE BEAMLINE

To validate that the achromat conditions are good proxies for the medical quality requirements, we study the five-magnet beamline shown in Fig. 1 for the case of 1 % momentum acceptance. The dipoles ($D_{15°}$) have a fixed strength to provide an overall bend of 30° for the reference energy trajectory. The other magnets are focusing and defocusing quadrupoles with gradients B_f and B_d. Due to the midpoint symmetry, these are the only free parameters. To limit the input value space, the first and last quadruple are set to be focusing, while the central one defocuses. Magnet and drift lengths (both 10 cm) are held constant to further reduce the degrees of freedom.

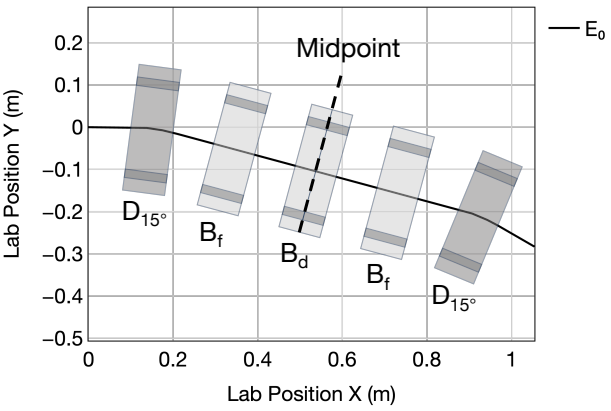

Figure 1: Five-magnet sample beamline.

For this simple case, it is possible to model the beamline with a simulation tool and evaluate the metrics given via Eq. (3), Eq. (4) and Eq. (5) for a range of input values (B_f, B_d) by brute-force calculations. The tracking code Zgoubi [13] is employed for the simulations as it handles large momentum deviations correctly by integrating the Lorentz force directly. Having only two degrees of freedom also enables the visual representation of the three quality metrics for combinations (B_f, B_d), shown in the first row of Fig. 2.

Analogously, we can evaluate the cost functions defined in Eq. (1) and Eq. (2) derived from the achromaticity conditions. Comparing the plots in the second row of Fig. 2 to the ones above them, we find that geometrical achromaticity (F_1) is a good proxy for the position deviation, while ellipticity and size variation are minimized by meeting the optical

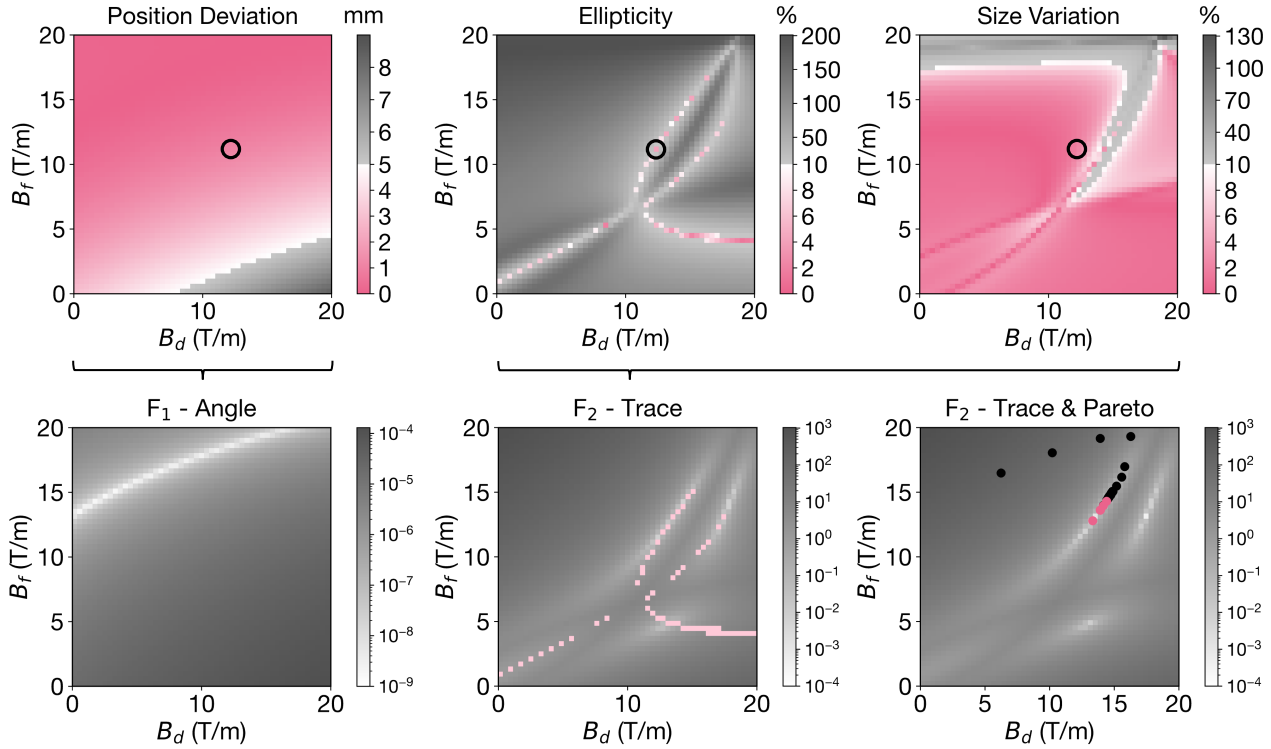

Figure 2: Quality metrics (first row) and achromaticity conditions (second row) evaluated for the sample beamline. A point (B_f, B_d) that is pink in all three of the upper plots – for instance the one highlighted by the black circles – relates to a suitable set of parameters meeting all requirements. In the central plot (F_2), light pink indicates allowed values according to the ellipticity and size variation metrics. In the right plot in the second row, the black and dark pink points show the parameters related to the Pareto optimization results with pink indicating combinations that meet all three quality metrics.

achromaticity condition (F_2). Most notably, the achromaticity conditions are not satisfied in the same regions, meaning that without any *a priori* knowledge of a correct weighting, they need to be optimized separately to then study the trade-off between them.

MULTI-OBJECTIVE ALGORITHM FOR SCALABLE PARAMETER OPTIMIZATION

For beamlines with more free parameters than the sample case discussed above, the computation time increases exponentially if we continue the brute-force exploration of the input value space. Given that the achromat conditions have been established as proxies for the beam quality metrics, a multi-objective algorithm can be used instead to find a set of optimal combinations (B_f, B_d), for which one of the cost functions (F_1, F_2) is only further minimized if the other one increases. This result is called a Pareto front. It describes the trade-off between the two achromaticity conditions and allows the selection of the most suitable parameters with respect to clinical quality requirements. Using the R-NSGA-II implementation provided by the Python library `pymoo` [14] as a multi-objective genetic algorithm, we determine the Pareto front for the five-magnet sample beamline. To evaluate the achromaticity conditions, we again use Zgoubi. The combinations (B_f, B_d) associated with the optimized cost functions are indicated via the black markers in the lower right plot of Fig. 2 and the results that stay within the allowed limits of all three quality metrics are shown in dark pink. We see that the Pareto technique finds solutions in one of the optimal regions previously validated by the brute-force calculations. As a next step, we plan to use this tool to explore beamlines with more components, for which we aim to limit the parameter space by creating a surrogate model based on transfer maps that allows faster initial computations.

CONCLUSION

In the context of charged particle therapy, we have described an approach to develop compact separate-function magnet beamlines. We have gathered clinical beam quality requirements, identified achromaticity conditions as proxies for them, and effectively expressed these metrics through accelerator physics concepts. We have investigated a five-magnet sample case to validate this relationship and to ensure that a multi-objective algorithm, which optimizes the achromaticity conditions, accesses the best parameter regions and provides suitable magnet settings facilitating consistent treatment. Next, we aim to extend our use of the multi-objective optimization to arcs composed of more magnets to investigate if relevant momentum acceptance ranges can be achieved with compact, separate-function beamlines.

REFERENCES

[1] K. J. Kirkby *et al.*, "Heavy charged particle beam therapy and related new radiotherapy technologies: The clinical potential, physics and technical developments required to deliver benefit for patients with cancer", *The British Journal of Radiology*, vol. 93, no. 1116, p. 20200247, Dec. 2020. doi:10.1259/bjr.20200247

[2] S. Yan, T. A. Ngoma, W. Ngwa, and T. R. Bortfeld, "Global democratisation of proton radiotherapy", *The Lancet Oncology*, vol. 24, no. 6, e245–e254, Jun. 2023. doi:10.1016/S1470-2045(23)00184-5

[3] R. Baskar, K. A. Lee, R. Yeo, and K.-W. Yeoh, "Cancer and Radiation Therapy: Current Advances and Future Directions", *Int. J. of Med.l Sci.*, vol. 9, no. 3, pp. 193–199, 2012. doi:10.7150/ijms.3635

[4] J. Yap, A. Steinberg, H. Norman, K. Nesteruk, and S. Sheehy, "Toward Ultra-fast Treatments: Large Energy Acceptance Beam Delivery Systems and Opportunities for Proton Beam Therapy", Jan. 2026, doi:10.48550/arXiv.2601.13577, arXiv: 2601.13577 [physics], (visited on 01/28/2026),

[5] J. Shen *et al.*, "Technical Note: Using experimentally determined proton spot scanning timing parameters to accurately model beam delivery time", *Medical Physics*, vol. 44, no. 10, pp. 5081–5088, Oct. 2017. doi:10.1002/mp.12504

[6] A. F. Steinberg, R. B. Appleby, J. S. L. Yap, and S. L. Sheehy, "Design of a large energy acceptance beamline using fixed field accelerator optics", *Phys. Rev. Accel. Beams*, vol. 27, no. 7, p. 071601, Jul. 2024. doi:10.1103/PhysRevAccelBeams.27.071601

[7] K. Halbach, "Design of permanent multipole magnets with oriented rare earth cobalt material", *Nucl. Instrum. Methods*, vol. 169, no. 1, pp. 1–10, Feb. 1980. doi:10.1016/0029-554X(80)90094-4

[8] K. P. Nesteruk, C. Calzolaio, D. Meer, V. Rizzoglio, M. Seidel, and J. M. Schippers, "Large energy acceptance gantry for proton therapy utilizing superconducting technology", *Physics in Medicine & Biology*, vol. 64, no. 17, p. 175007, Sep. 2019. doi:10.1088/1361-6560/ab2f5f

[9] H. Wiedemann, *Particle Accelerator Physics*. Cham, Springer, 2015. doi:10.1007/978-3-319-18317-6

[10] L. Grevillot *et al.*, "Clinical implementation and commissioning of the MedAustron Particle Therapy Accelerator for non-isocentric scanned proton beam treatments", *Medical Physics*, vol. 47, no. 2, pp. 380–392, Feb. 2020. doi:10.1002/mp.13928

[11] Y. Liao, R. Zhao, X. Liu, G. Chen, Q. Chen, and B. Qin, "High order beam optics optimization for a superconducting gantry applied to proton therapy based on NSGA-III", *Nucl. Instrum. Methods Phys. Res., Sect. A*, vol. 1014, p. 165727, Oct. 2021. doi:10.1016/j.nima.2021.165727

[12] B. Arjomandy *et al.*, "AAPM task group 224: Comprehensive proton therapy machine quality assurance", *Medical Physics*, vol. 46, no. 8, Aug. 2019. doi:10.1002/mp.13622

[13] F. Méot, "The ray-tracing code Zgoubi", *Nucl. Instrum. Methods Phys. Res., Sect. A*, vol. 427, no. 1-2, pp. 353–356, May 1999. doi:10.1016/S0168-9002(98)01508-3

[14] https://pymoo.org/algorithms/moo/rnsga2.html (visited on 04/26/2026),